J. Phys.: Condens. Matter 4 (1992) 9673–9696. Printed in the UK

Magnetic structures and interactions in erbium

R A Cowley† and J Jensen‡

† Oxford Physics, Clarendon Laboratory, Parks Road, Oxford OX1 3PU, UK
‡ Physics Laboratory, Universitetsparken 5, 2100 Copenhagen, Denmark

Received 20 August 1992

Abstract. The magnetic structures in a single crystal of isotopically enriched erbium have been studied using a high-resolution neutron diffraction technique at the HFIR reactor at Oak Ridge National Laboratory. In addition, these structures have been examined by mean-field calculations, in which the primary interactions were derived from magnetization and spin-wave measurements. The agreement between theory and experiment is generally very good. At intermediate temperatures, the structure is based on an elliptical cycloid in the a–c plane, and blocks of moments with alternating positive and negative components in the c-direction give rise to a series of commensurable structures in the manner proposed by Gibbs and co-workers. These structures are, however, distorted by two-ion couplings of trigonal symmetry, which reflect the different orientation of the two HCP sublattices and have a magnitude which is a substantial fraction of the isotropic exchange interaction. The result is a wobbling cycloid, in which there is an oscillating moment in the b-direction whose period differs from that of the basic cycloidal structure. In the low-temperature cone phase, the moments bunch around alternating a-directions in a pattern with trigonal rather than hexagonal symmetry. Some further consequences of the trigonal couplings on the low-symmetry magnetic structures in erbium and holmium are discussed.

1. Introduction

The first thorough study of the magnetic ordering in erbium was performed by Cable *et al* (1965), using neutron diffraction. They reported three distinctly different magnetically ordered phases which can be briefly described as follows.

(i) Between $T_N = 84$ K and $T_N' = 52$ K, a sinusoidal ordering of the longitudinal c-components of the magnetic moments, with a period of approximately three and a half lattice spacings along the c-axis of the HCP lattice.

(ii) Between T_N' and $T_C = 18$ K, the wavevector of the modulated phase q_c decreases from $\frac{2}{7}\tau_c$ to $\frac{1}{4}\tau_c$, and there is ordering of both the basal-plane and longitudinal spin components (τ_c is the reciprocal lattice vector along the c-axis of length $\tau_c = 2\pi/c$).

(iii) Below T_C, the magnetic structure is a cone with a ferromagnetic moment along the c-axis, and a basal-plane component with a modulation wavevector of $\frac{5}{21}\tau_c$.

In 1974 more refined studies were made (Habenschuss *et al* 1974, Atoji 1974) and phases (i) and (ii) showed higher harmonics of the modulation wavevector, the intensities of which tended to increase with decreasing temperature. Later Gibbs *et al* (1986) performed a high-resolution synchrotron x-ray study, and found in the intermediate phase (ii) a number of long-period commensurable structures with wavevectors $\frac{1}{4}$, $\frac{6}{23}$,

0953-8984/92/489673+24$07.50

$\frac{5}{19}$, $\frac{4}{15}$ and $\frac{2}{7}\tau_c$. Most recently Lin *et al* (1992) have investigated the magnetic phase diagram of erbium in a c-axis magnetic field by neutron diffraction experiments.

The main purpose of this paper is to provide an improved picture of these structures, particularly in the intermediate phase (ii), by using both neutron scattering and theoretical calculations. Magnetic x-ray scattering techniques provide very good resolution, but the intensity is weak, preventing the determination of the intensities of the weak reflections. In contrast, neutron diffraction reflections have high intensities, although the resolution is relatively poor, and the use of a large single crystal and a triple-axis spectrometer makes it possible to detect most of the scattering peaks originating from the long-period commensurable structures, as illustrated by the study of spin-slips in holmium (Cowley and Bates 1988). We have used very similar techniques in these experiments.

The most important magnetic interaction in erbium, and in the other heavy rare-earth metals, is the isotropic RKKY exchange interaction $\mathcal{J}(ij)$ between the localized moments, which is long-ranged and oscillates in magnitude. If anisotropy effects can be neglected, this two-ion coupling leads to a modulated structure with the wavevector q_c at which the Fourier transform $\mathcal{J}(q)$ has its maximum. The free energy is minimized when the length of the ordered moments on different sites is constant, and the magnetic structures therefore consist of ferromagnetic sheets perpendicular to the c-axis, with the moments rotating through a certain angle, as determined by q_c, from one sheet to the next. The crystalline anisotropy in the HCP structure favours either a longitudinal (along the c-axis) or transverse (perpendicular to the c-axis) alignment of the magnetic moments. In the latter case, as found in holmium, the magnetic structure is a helix which is distorted at low temperatures by the hexagonal anisotropy, with higher harmonics at the wavevectors $(6 \pm 1)q_c$. In the former case, the magnetic structures depend on the strength of the anisotropy. The longitudinal component orders at T_N, and if the axial anisotropy is sufficiently large, as occurs in thulium, the ordering of the transverse components is entirely suppressed, but the longitudinal wave squares up to form a structure in which the magnitude of the ordered moments varies as little as possible. If the axial anisotropy is weaker, mean-field analyses (Miwa and Yosida 1961, Nagamiya 1967, Jensen 1976) indicate that ordering of the longitudinal component will be followed, at a lower temperature T_N', by ordering of one of the two basal-plane components of the moments, to produce an elliptical cycloidal structure in which the moments are aligned in a plane containing q_c. As the temperature is lowered further, there is a competition between the squaring of the longitudinal ordering, to reduce the anisotropy energy, and the reduction of the eccentricity of the ellipsoidal ordering, to reduce the exchange energy.

In the case of the intermediate phase (ii) in erbium, the nature of the ordering has been the subject of some controversy. Cable *et al* (1965) suggested from their neutron diffraction measurements that both basal-plane components ordered at T_N' in a helical structure. Unfortunately, the scattering from random domains of this non-planar structure, and from random domains of the cycloidal structure are qualitatively very similiar. The Landau expansion of the free energy predicts, however, that the non-planar structure is unstable compared to the cycloidal structure, at least close to T_N', because the variation in the length of the moments is more effectively minimized by the cycloidal arrangement than in the non-planar structure. The remaining basal-plane component may order in a continuous way, at a lower temperature, if higher-rank anisotropy effects tilt the direction of the easy axis away from the c-axis, but there are no indications of such an additional second-order transition in erbium. The

diffraction experiments reported below did not reveal any difference between the ordering wavevectors of the c-component and of the basal-plane components in the intermediate phase, and they gave a strong *third* harmonic in the modulation of the basal-plane moments. Both observations indicate that the longitudinal and the basal-plane components are phase locked, and hence that erbium is ordered in a cycloidal structure between T_N' and T_C.

The commensurable structures in phase (ii) observed by Gibbs *et al* (1986) arise because the anisotropy favours a large component of the ordered moments along the c-axis. Just below T_N', the structure is similar to the commensurable thulium structure, with four hexagonal layers in which the moments have a positive c-component, followed by three layers of moments with a negative c-component. The ordering wavevector is $q_c = \frac{2}{7}\tau_c$, and this structure may be designated as (43). However, the HCP structure has two inequivalent sublattices so that the magnetic structure repeats after every fourteen magnetic layers, rather than seven, so a more appropriate description is (4343) or 2(43). Below T_N', the ordering wavevector decreases with decreasing temperature, and the system traverses a series of commensurable structures, in which more and more of the bunches of three moments are replaced by bunches of four moments, giving $2(43) \rightarrow 2(443) \rightarrow 2(4443)$ etc. until, just above T_C, the magnetic structure reaches (44), with a periodicity of eight layers and $q_c = \frac{1}{4}\tau_c$.

In this paper, we present a detailed description of these structures, and of the low-temperature cone structure, on the basis of both experiment and theory. In the next section, we summarize the neutron scattering measurements, which were performed at the HFIR reactor at the Oak Ridge National Laboratory, USA. In section 3 a mean-field model for erbium is introduced, similar to that used earlier (Jensen 1976), but extended to include a two-ion coupling with trigonal symmetry between the different sublattices, introduced in order to explain the observed period doubling of the magnetic structures. In section 4 the experimental diffraction results are analysed and compared with the predictions of the mean-field calculations. Our conclusions concerning the magnetic structures of erbium, and a general discussion of the effects produced by the trigonal coupling are presented in section 5.

2. Experimental results

The neutron scattering measurements were performed with the HB3 triple-axis crystal spectrometer at the HFIR reactor. Pyrolytic graphite was used as monochromator and analyser and the horizontal collimation was 20′–20′–20′, open from reactor to counter. The incident neutron energy was fixed at 14.8 meV, and a pyrolytic graphite filter was used to reduce the higher-order contaminent neutrons. The wavevector resolution was typically 0.01–0.02 reciprocal lattice units and the spectrometer was operated so as to measure the elastic scattering with wavevector transfers $(00L)$, $(10L)$ and $(20L)$ in reciprocal space.

The sample of erbium was the same isotopically enriched crystal as that used in earlier inelastic studies (Nicklow *et al* 1971) and was mounted in a variable temperature cryostat with the scattering plane of the spectrometer normal to (010). The temperature could be held fixed to ±0.1 K, and there was little evidence of hysteresis in the results on heating or cooling.

Typical results are shown in figure 1 for scans along both $[00L]$ and $[10L]$, with the intensity plotted on a logarithmic scale. There is clearly a series of regular peaks

in intensity corresponding to a periodicity of $\frac{1}{15}\tau_c$, with the largest peaks occurring at $q_c = \frac{4}{15}\tau_c$. The scattering may therefore be deduced to arise from the 2(4443) structure, and the large number of peaks shows that the structure is far from sinusoidal. Similar measurements were performed at other temperatures and the positions of the peaks are shown in figure 2. At lower temperatures, the wavevector corresponds to a long-period commensurable structure, but above about 40–50 K, the structure is incommensurable, though close to either 2(43) or 2(443). We have therefore chosen to analyse these structures as though they were the nearest commensurable structure. The smallest separation of the peaks determines the basic ordering periodicity, q_0, and the ratio $r = q_c/q_0$ gives the number of times the ordered moments rotate in one commensurable period. The different structures are listed in table 1.

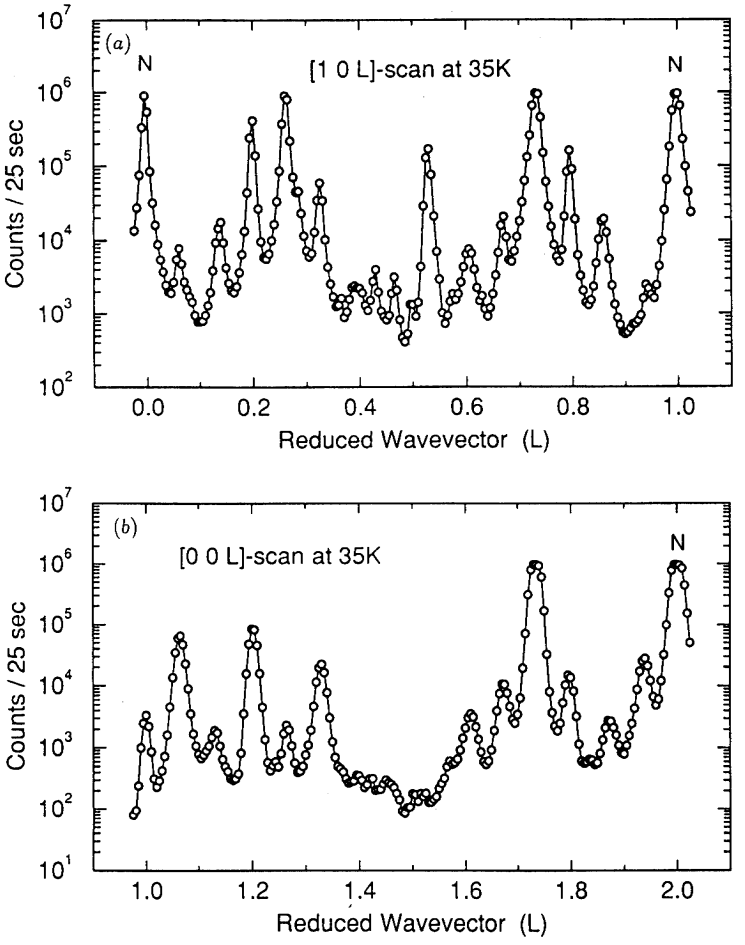

Figure 1. The neutron scattering observed from erbium at 35 K. The left-hand panel of the figure shows a scan along $[10L]$ and the right-hand one along $[00L]$. The peaks marked N are from nuclear scattering and the remainder are magnetic in origin.

Further information about the structures can be obtained from the intensities of the peaks. These are however difficult to measure and subject to significant errors. Firstly, the data were corrected for the instrumental effects arising in obtaining integrated

Table 1. Commensurable structures.

T (K)	Structure	q_0 (τ_c)	q_c (τ_c)
54, 49	2(43)	1/7	2/7
44, 40	2(443)	1/11	3/11
35	2(4443)	1/15	4/15
29	2(44443)	1/19	5/19
25	2(444443)	1/23	6/23
20	(44), (3030)	1/4	1/4

intensities from triple-axis spectrometer scans along $[00L]$ and $[10L]$ lines in reciprocal space (Cowley and Bates 1988). Secondly, the data were corrected for the wavevector dependence of the magnetic form factor. Since the crystal was isotopically enriched and of complex shape, no corrections were made for its neutron absorption. This is at least in part justified because equivalent intensities obtained at different wavevector transfers did agree with one another to within about a factor of 2. More difficult are the problems of extinction and of multiple scattering. Since our objective was to measure the weak reflections, we used a large crystal and there is no doubt that our data suffer from both of these problems. We treated the extinction problem by comparing our results with those of Habenschuss *et al* (1974), whose intensities were much lower and consequently less affected. The higher-order reflections (third and fifth harmonics) in the two experiments were scaled to one another, and the intensities of the primary satellites then deduced from their data. This gave considerably more intensity for the primary reflections than we actually measured, and provides a more satisfactory measure of the correct intensity. In the analysis described below we have used these 'corrected' intensities. Multiple scattering can give large errors in modulated structures and this was studied by rotating the crystal around the scattering vector, and by comparing the intensities observed at equivalent points in reciprocal space. By using these approaches, we obtained a list of the best estimates for the intensities for the different peaks observed in the scans. These intensities, which vary over about four orders of magnitude, are uncertain by factors of the order of 2 or 3, but they can nevertheless be used to determine the detailed structures.

The different peaks shown in figures 1 and 2 can be classified as odd harmonics of the primary reflections, and the intensities in the $[10L]$ scans decrease systematically with the rank of the harmonic. The intensities of the peaks in these scans are dominated by the longitudinal components of the ordered moments. The corresponding results for the $[00L]$ scans, figures 1 and 2, arise from the scattering by the transverse or basal-plane components of the ordered moments. It is clear that the same harmonics occur as in the longitudinal ordering, which reflects the strong phase coherence between the two components. This is incompatible with a helical ordering of the basal-plane moments and is strong evidence for a cycloidal phase (Jensen and Mackintosh 1991). An unexpected feature of the $[00L]$ scans is the observation of higher harmonics at the wavevectors $q = \pm(2p + 1)q_c + n\tau_c$ with n odd, as well as even. These peaks with n odd would be absent in the scattering from a planar cycloidal structure, in which both of the hexagonal sublattices are equivalent. They are also unusual in that the intensities are largest for the third and fifth harmonics. As we shall demonstrate below, these results show that there is a large two-ion coupling with trigonal symmetry in erbium, which modifies the planar cycloid into a non-planar wobbling cycloidal structure.

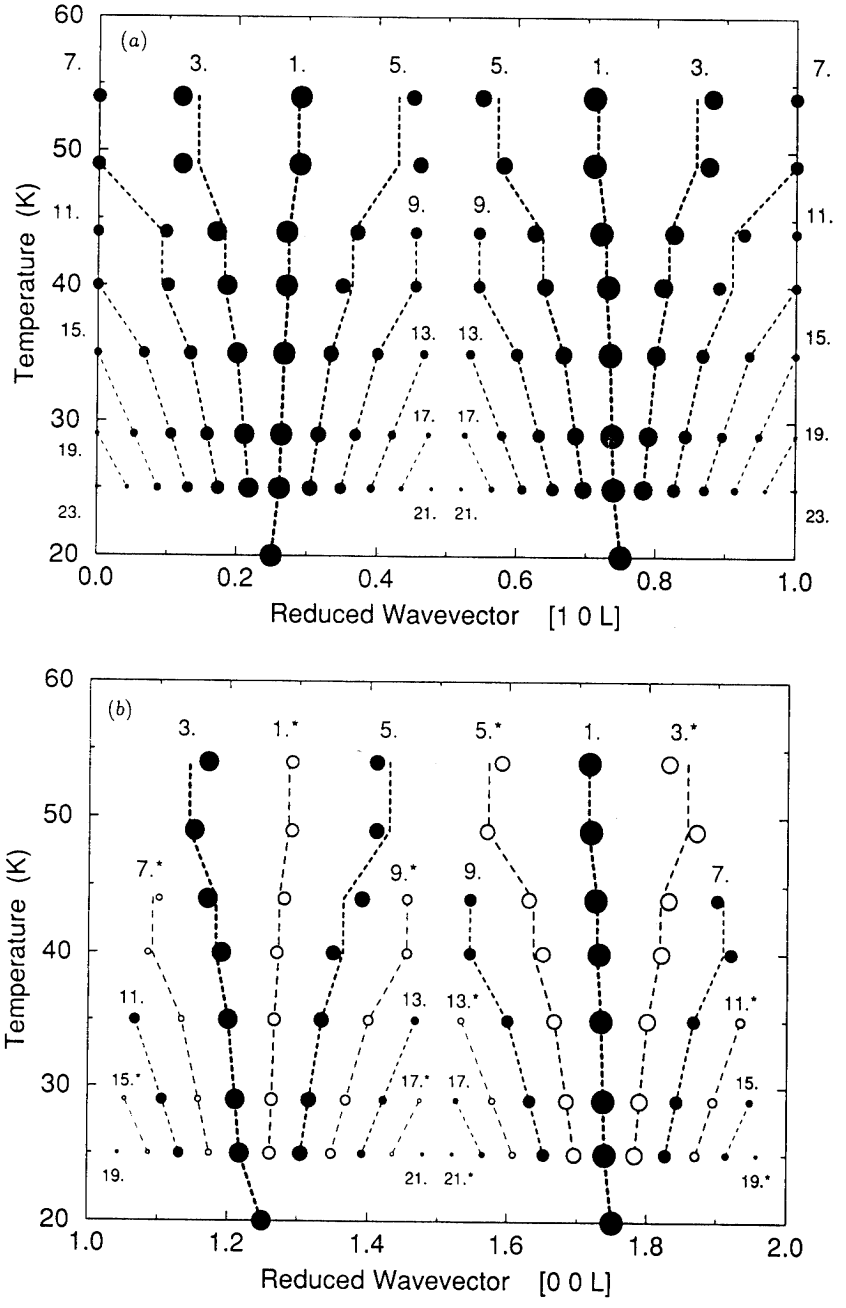

Figure 2. (*a*) A schematic plot of the positions at which peaks have been observed in the $[10L]$ scans, indicating the relative intensities by the size of the dots. The different peaks are classified as higher odd harmonics of the fundamental, i.e. by the number $(2p+1)$ which relates their position at $q = \pm(2p+1)q_c + n\tau_c$ (p and n are integers and $p \geqslant 0$) with the position of the main peak at q_c. The magnetic contributions to the Bragg peaks at (100) and (101) were not determined, but the expected harmonics at the two positions are included in the figure. (*b*) A similar plot derived from the $[00L]$ scans. In the classification of the harmonics, the asterisk indicates those which correspond to odd values of n, and would not be present in the absence of the trigonal coupling which distinguishes between the two sublattices of the HCP structure. A few of the lowest-intensity peaks in this plot, for $T \leqslant 35$ K, were too weak to be observed, but are included in the figure for completeness.

3. The mean-field model

The model which we have adopted for erbium is similar to that used earlier (Jensen 1976). The Hamiltonian includes the single-ion anisotropy, the Heisenberg exchange interaction, the classical magnetic dipole–dipole coupling, and an anisotropic two-ion interaction indicated by the spin-wave dispersion relation. The Hamiltonian is then

$$\mathcal{H}_0 = \sum_i \sum_{lm} B_l^m O_l^m(i) - \tfrac{1}{2} \sum_{ij} \mathcal{J}(ij) \boldsymbol{J}_i \cdot \boldsymbol{J}_j - \tfrac{1}{2} \sum_{ij} \mathcal{J}_D(ij) J_{zi} J_{zj} - \tfrac{1}{2} \sum_{ij} K_{33}^{2-2}(ij) [O_3^2(i) O_3^2(j) + O_3^{-2}(i) O_3^{-2}(j)]. \tag{1}$$

The x-, y-, and z-axes are along respectively the a-, b- and c-axes of the HCP lattice. The Stevens operators are $O_3^{\pm 2} = \frac{1}{2}(J_z O_2^{\pm 2} + O_2^{\pm 2} J_z)$, where $O_2^2 = J_x^2 - J_y^2$ and $O_2^{-2} = J_x J_y + J_y J_x$. The Fourier transform of $\mathcal{J}(ij)$ is

$$\mathcal{J}(\boldsymbol{q}) = \frac{1}{N} \sum_{i,j} \mathcal{J}(ij) \, \mathrm{e}^{-\mathrm{i}\boldsymbol{q}\cdot(\boldsymbol{R}_i - \boldsymbol{R}_j)} \tag{2}$$

where N is the number of ions in the crystal, and we use $\mathcal{J}(q)$ as a short-hand notation for $\mathcal{J}(\boldsymbol{q})$ when $\boldsymbol{q}$ is parallel to the c-axis. Analogous quantities may be defined for the other two-ion couplings.

The dipolar contribution to the coupling of the basal-plane moments is included in $\mathcal{J}(q)$. The coupling of the c-components is $\mathcal{J}_{cc}(q) = \mathcal{J}(q) + \mathcal{J}_D(q)$, with

$$\mathcal{J}_D(q) = -\mathcal{J}_{dd}\{0.919 + 0.0816\cos(qc/2) - 0.0006\cos(qc)\} \tag{3}$$

when q is non-zero, and $J_D(0) \equiv 0$. The coupling constant

$$\mathcal{J}_{dd} = 4\pi(g\mu_B)^2 N/V = 0.0316\,\mathrm{meV}$$

where V is the volume of the crystal.

The axial anisotropy B_2^0 is obtained from the high-temperature susceptibilities shown in figure 3, which determine $\mathcal{J}(0) = 0.207\,\mathrm{meV}$ and, from the value of T_N, $\mathcal{J}(q_c) + \mathcal{J}_D(q_c) = 0.286\,\mathrm{meV}$. In the analysis of the susceptibility and the low-temperature magnetization, we have included a contribution from the polarization of the conduction electrons of 3%, which value, being proportional to $(g-1)/g$, corresponds to the 9% increase of the saturation magnetization observed in Gd. The two remaining axial anisotropy parameters, B_4^0 and B_6^0, are determined from the magnetization along the c-axis in the cone phase at zero field, and its variation with field along the c-axis, shown in figure 4. The hexagonal anisotropy B_6^6 favours an alignment of the moments in the basal plane and is important, for instance, for the low-temperature transition to an a-axis magnet, observed when a field is applied along this axis. The point-charge model predicts $B_6^6 = -\frac{77}{8} B_6^0$, and the best fit was obtained using a value of B_6^6 about 25% smaller than indicated by this relation. The final crystal-field parameters used in the model are given in table 2.

The inter-planar exchange parameters $\mathcal{J}_n$ are defined by

$$\mathcal{J}(q) = \mathcal{J}_0 + 2 \sum_{n \geqslant 1} \mathcal{J}_n \cos(nqc/2) \tag{4}$$

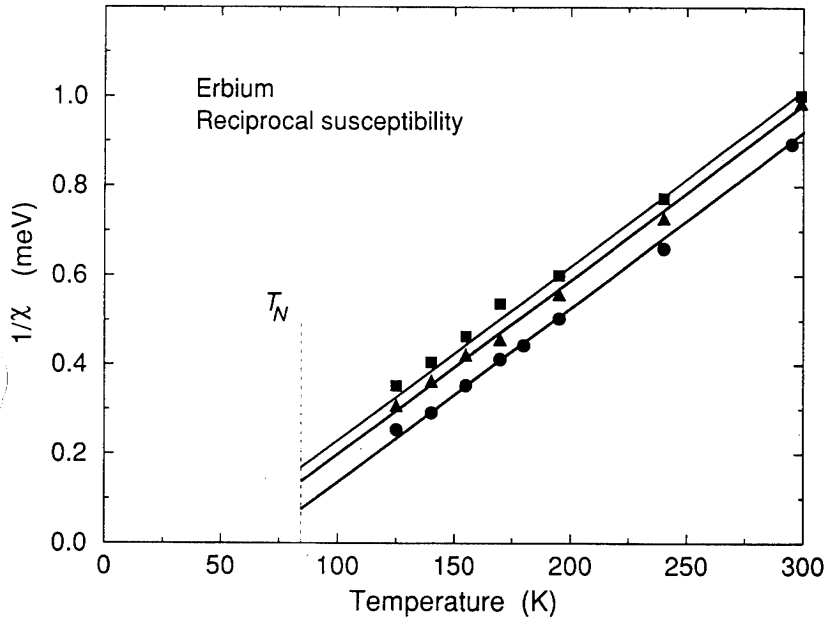

Figure 3. The reciprocal susceptibilities of paramagnetic erbium as a function of temperature. The solid curves are calculated and the experimental data are taken from Green *et al* (1961). The upper and lower results (squares and circles) refer respectively to a field perpendicular or parallel to the c-axis. The triangles are the average obtained from a polycrystalline sample.

and the anisotropic two-ion interaction parameters $[K_{33}^{2-2}]_n$ are defined similarly. The high-temperature susceptibilities, the value of T_N and of q_c (at T_N) lead to three constraints on the $\mathcal{J}_n$. The remaining parameters, determining $\mathcal{J}(q)$ and $K_{33}^{2-2}(q)$, are derived from the experimental spin-wave energies in the cone phase (Nicklow *et al* 1971). In our analysis, the spin-wave energies were calculated numerically within the MF–RPA approximation, without making use of the large-J approximation underlying the usual linear spin-wave theory. A detailed account of the theory has been given by Jensen and Mackintosh (1991) and by McEwen *et al* (1991). Nicklow *et al* (1971) and Jensen (1976) showed, using linear spin-wave theory, that it is impossible to explain the variation of the energies and scattering intensities of the c-axis spin waves observed in the conical phase of erbium, if the two-ion anisotropy is neglected. This conclusion is not changed when we apply the more accurate theory. The linear spin-wave theory neglects higher-order $1/J$-renormalization effects, and the anisotropic component $K_{22}^{2-2}(q)$ (Jensen 1974, 1976), is multiplied by an overall scale factor of about 1.6, compared with the estimate based on the linear theory. However, the present analysis indicates that including $K_{33}^{2-2}(q)$, rather than $K_{22}^{2-2}(q)$, gives a better overall account of the magnetic properties of erbium. Both kinds of anisotropy have similar effects on the spin waves, but they modify the cycloidal structures slightly at elevated temperatures in different ways, and $K_{22}^{2-2}(q)$ suppresses strongly the transition to the a-axis magnet, when a field is applied along this direction, in contradiction with the experimental behaviour shown in figure 4.

The final inter-planar coupling parameters are given in table 3, and the intra-

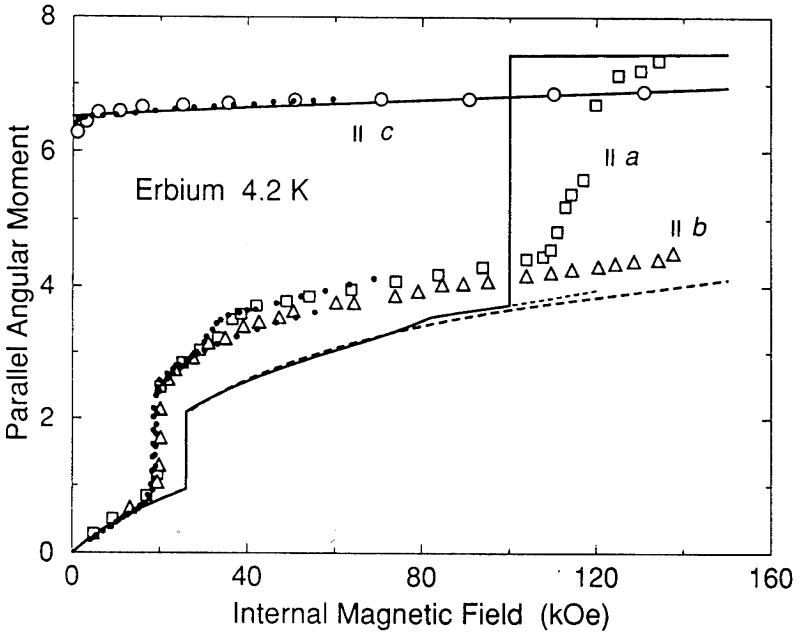

Figure 4. The magnetization curves in erbium at 4.2 K. The figure shows the average component parallel to the field of the site-dependent angular moments, $\langle J_{\parallel} \rangle$, as a function of the internal magnetic field applied along the three symmetry-directions. The solid curves display the MF results, and the experimental points are taken from Bozorth *et al* (1972), which are consistent with the results obtained by Féron (1969) (see also Coqblin 1977) below 60 kOe, shown by the black dots (his c-axis data are obtained at 20 K, where the slope is expected to be slightly larger than at 4.2 K). The saturation value of the magnetization, when $\langle J_{\parallel} \rangle = 7.5$, is assumed to be 310 emu g^{-1} including a 3% increase due to the polarization of the conduction electrons.

Table 2. Crystal-field parameters (meV).

B_2^0	B_4^0	B_6^0	B_6^6
-0027	-0.3×10^{-4}	0.13×10^{-5}	-0.9×10^{-5}

planar coupling $[K_{33}^{2-2}]_0$ is chosen to be zero (Jensen 1976). The corresponding results for the spin-wave energies are shown in figure 5. In addition, the calculated scattering intensities of the spin waves are in agreement with the previous theory and hence with experiment (Jensen 1974). The two exchange coupling parameters, $\mathcal{J}(q)$ and $\mathcal{J}_{cc}(q) = \mathcal{J}(q) + \mathcal{J}_D(q)$, are compared with the effective two-ion anisotropy

$$\mathcal{K}(q) = (J - \tfrac{1}{2})^2 (J - 1)^2 K_{33}^{2-2}(q) \qquad (5)$$

in figure 6. In terms of $\mathcal{K}(q)$ the (leading-order) contribution to the cone-energy at zero temperature is $-\frac{1}{2} N J^2 \mathcal{K}(2q_c) \cos^2\theta \sin^4\theta$. A comparison of the magnitude of the different couplings involves some arbitrariness. The anisotropy component depends on the direction of magnetization ($\cos^2\theta \sin^4\theta \simeq 0.04$), and the comparison may be based on the energy contribution, as here, or on the effects on the excitation

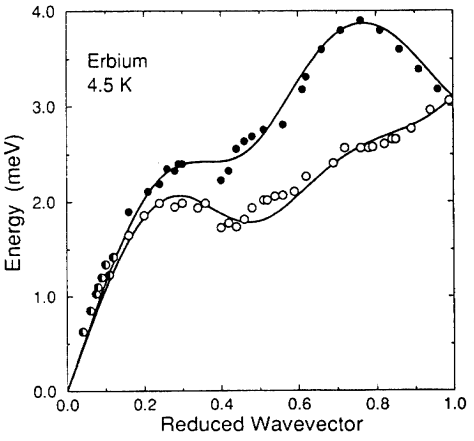

Figure 5. Spin-wave dispersion relations in the c-direction in the cone phase of erbium at 4.5 K. The closed and open circles represent the measured $+q$ and $-q$ branches, respectively (Nicklow *et al* 1971). The solid lines are the results of the MF-RPA calculation.

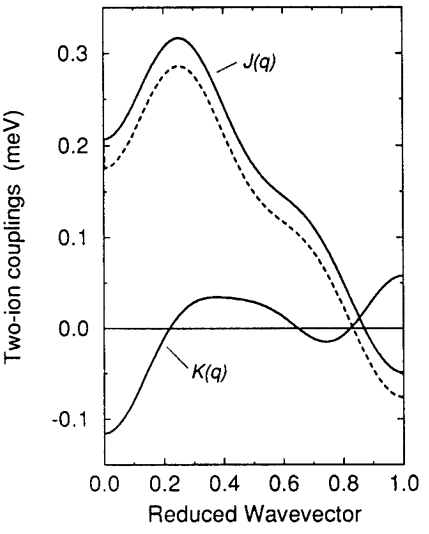

Figure 6. The Fourier transform of the two-ion couplings in erbium as determined from the inter-planar coupling coefficients given in table 3. $\mathcal{J}(q)$ and $\mathcal{J}_{cc}(q)$ (the dashed line) and the anisotropy component $\mathcal{K}(q)$ are plotted as functions of the reduced wavevector q/τ_c, along the c-axis.

Table 3. Inter-planar coupling parameters (meV).

n	0	1	2	3	4	5
$\mathcal{J}_n$	0.165	0.073	−0.025	−0.006	−0.018	−0.003
$\left[K_{33}^{2-2}\right]_n \times 10^5$	0.0	−0.8	−0.7	-1.0	0.0	−0.3
$\left[K_{31}^{21}\right]_n \times 10^3$	0	0.6	−0.25	−0.05		

energies, as considered previously (Jensen 1976), in which case the effective $\mathcal{K}(q)$ is a factor of 4 larger than the function defined in (5).

The general arguments presented in the appendix show that the symmetry of the HCP lattice allows two-ion couplings which change sign when the sublattices are interchanged, or when the crystal is rotated 60° around the c-axis. To lowest order there are three possibilities, and the one which most readily accounts for the measurements is

$$\mathcal{H}_3 = \sum_{ij} K_{31}^{21}(ij)\left[O_3^2(i)J_{yj} + O_3^{-2}(i)J_{xj}\right]. \tag{6}$$

We therefore take the total Hamiltonian as $\mathcal{H} = \mathcal{H}_0 + \mathcal{H}_3$.

The two-ion couplings are treated in the mean-field approximation, so that the MF Hamiltonian for the ith ion, $\mathcal{H}_{MF}(i)$, includes the exchange term

$$-(\boldsymbol{J}_i - \tfrac{1}{2}\langle \boldsymbol{J}_i\rangle)\cdot\sum_j \mathcal{J}(ij)\langle \boldsymbol{J}_j\rangle.$$

According to the general relations derived in the appendix, the contribution of $\mathcal{H}_3$ to $\mathcal{H}_{MF}(i)$ is given by

$$\begin{aligned}\Delta\mathcal{H}_{MF}(i \in p\text{th plane}) = (-1)^p \sum_{n\geqslant 1} [K_{31}^{21}]_n \\ \times \Big[\{O_3^2(i) - \tfrac{1}{2}\langle O_3^2(i)\rangle\}\langle J_y(p+n) - J_y(p-n)\rangle \\ + \{O_3^{-2}(i) - \tfrac{1}{2}\langle O_3^{-2}(i)\rangle\}\langle J_x(p+n) - J_x(p-n)\rangle \\ - (-1)^n\{J_{yi} - \tfrac{1}{2}\langle J_{yi}\rangle\}\langle O_3^2(p+n) - O_3^2(p-n)\rangle \\ - (-1)^n\{J_{xi} - \tfrac{1}{2}\langle J_{xi}\rangle\}\langle O_3^{-2}(p+n) - O_3^{-2}(p-n)\rangle\Big]\end{aligned} \tag{7}$$

where the argument $p \pm n$ denotes an ion in the $(p \pm n)$th hexagonal layer. Table 3 gives the values used for the inter-planar coupling constants $[K_{31}^{21}]_n$, which were obtained by comparison of the calculated and observed neutron diffraction intensities.

The structures were calculated by a straightforward iteration procedure. The first step was to assume a distribution of the expectation values of the various operators, and to insert these values in the MF Hamiltonian for the ith ion, which was then diagonalized. The partition function, the free energy, and new expectation values for this ion could then be calculated. By carrying out this calculation for all the different ions in one commensurable period, we obtained a new distribution of expectation values, and the procedure was then repeated until self-consistency was obtained. The convergence is reasonably rapid except close to a second-order transition. In the calculations, the length of the commensurable period was considered fixed, so that the derived structures are generally only metastable. Except for the specification of the length of the commensurable period and the main characteristics of the structure, e.g. whether the arrangement is cycloidal or conical, the structures given by the model are independent of the starting distribution.

The trigonal coupling was included in all the structure calculations, but estimates showed that it is unimportant in the calculation of the spin-wave dispersion relation. This is also the case for the single-ion hexagonal anisotropy B_6^6, and both were neglected in the spin-wave calculations of figure 5. These interactions have a slight influence on the mean opening angle θ of the cone, which was accounted for by a small adjustment of B_4^0 in the spin-wave calculation, and also lead to off-diagonal interactions between spin-waves at different q-values. The second-order effects on the spin waves are small, and the first-order energy gaps, which occur whenever the spin-wave energies $\varepsilon(q) = \varepsilon(\pm q \pm 3q_c + \tau_c)$ or $\varepsilon(q) = \varepsilon(\pm q \pm 6q_c)$, are estimated to be of the order of 0.1 meV, which is too small to have been resolved in the experiments. Such gaps do not coincide with the two gaps indicated by the experiments close to $q = \pm 0.4\tau_c$, which may rather be explained as originating from a threefold symmetric interaction between the spin waves and the transverse phonons (Jensen and Houmann 1974, Jensen and Mackintosh 1991).

The model developed here has the same deficiencies in describing erbium at low temperatures as the earlier one (Jensen 1976); the cone phase has too high an energy and the fit to the basal-plane magnetization curves at 4.2 K is unsatisfactory. The calculated energy of the cone phase lies about 1 meV/ion above that of the cycloidal phase in the zero-temperature limit. Part of the discrepancy arises from the two-ion magnetoelastic effects, and the α-strain changes occurring at T_C account for about 0.2 meV/ion (Rosen

et al 1973, Jensen and Mackintosh 1991). In the calculation of the low-temperature magnetization curves in figure 4, we have neglected the more stable phase, in which the c-axis moments oscillate between positive and negative values, as being an artefact of the model. The agreement with experiment is good when the field is applied along the c-axis, and also at low fields, but not at high fields, in the basal plane. The model accounts correctly for the *effective* anisotropy in the zero-field cone phase.

The a-axis magnetization data (Bozorth *et al* 1972, Féron 1969) show two low-field transitions, at about 20 and 35 kOe. The calculations indicate that the system is in the fan phase between the two transitions, and that it is ferromagnetic above the second. Around 120 kOe, the angle between the direction of the ferromagnetic moments and the c-axis changes abruptly from $\sim 35°$ to 90°. In the case where the field is applied along the hard axis in the basal plane, the b-axis, the fan phase appears to be stable from about 20 kOe up to the maximum field of about 140 kOe.

The discrepancies between the results predicted by the model and the experimental data indicate that it is incomplete. We have already mentioned that the α-strain two-ion couplings tend to stabilize the cone phase. All the strains influence the basal-plane magnetization, but the magnetoelastic changes are estimated to be too small to explain all the deficiencies. We have neglected any variation of the coupling parameters with temperature, although the temperature dependence of the ordering wavevector suggests such an effect, which has also been observed in other rare earths (Jensen and Mackintosh 1991). The RKKY exchange coupling may change due to the deformation of the Fermi surface of the conduction electrons induced by the polarization of the local moments, or, as proposed recently by Plumer (1991) for the case of holmium metal, because of two-ion magnetoelastic effects. In addition, the analysis of the spin-wave dispersion relation does not exclude the possibility that other axial anisotropic two-ion couplings, besides the classical dipole term, are present. As discussed earlier (Jensen 1976), these couplings do not influence the spin waves very much but may be important for the structural energies. It is possible to remove the two specific discrepancies mentioned above by allowing the difference $\mathcal{J}(q_c) - \mathcal{J}(0)$ to be temperature dependent, assuming the low-temperature value to be about a factor of two smaller than that derived from the high-temperature properties. However, this more complex model has other deficiencies, as the descriptions of the spin-wave energies and of the magnetic structures in the intermediate phase become less satisfactory. All in all, these features indicate that a more realistic model for erbium than the one presented here should include the magnetoelastic effects, a temperature variation of $\mathcal{J}(q)$, and additional axial two-ion anisotropy. Although the existence of various possibilities for the anisotropic two-ion couplings in erbium may introduce some arbitrariness in the derivation of the isotropic exchange coupling from the spin-wave data, the $\mathcal{J}(q)$ of figure 6 is close to that obtained earlier, indicating that it is quite insensitive to the assumed form of the anisotropy.

4. The commensurable magnetic structures

The magnetic structures of erbium have been determined in two different ways. Firstly, the mean-field theory described in section 3 has been used to calculate them. The structure is specified by $\langle J_p \rangle$, where p is a label of one of the m different layers in a commensurable period. The static correlation function is then given by

$$S_{\alpha\alpha}(\kappa) = \left| \frac{1}{N} \sum_j \langle J_{\alpha j} \rangle \, e^{iR_j \cdot \kappa} \right|^2 \tag{8}$$

We assume an equal distribution of domains, so that terms in the cross-section which are either off-diagonal or odd with respect to κ cancel. The scattered intensity is proportional to the components of the moments perpendicular to the wavevector transfer, so that

$$I(00L) = S_{xx}(\kappa) + S_{yy}(\kappa) \tag{9}$$

with $L = q/\tau_c$, while

$$I(10L) = (1 - \tfrac{1}{2}\hat{\kappa}_\perp^2)[S_{xx}(\kappa) + S_{yy}(\kappa)] + (1 - \hat{\kappa}_\parallel^2) S_{zz}(\kappa) \tag{10}$$

where $\hat{\kappa}_\perp$ and $\hat{\kappa}_\parallel$ are respectively the component of the unit vector κ/κ perpendicular and parallel to the c-axis.

When κ is parallel to the c-axis, the scattering function does not depend on the orientation of the two sublattices and equation (8) is identical to that which would be derived for a simple hexagonal lattice with the smallest effective reciprocal lattice vector of $2\tau_c$. Similarly, in the absence of the trigonal interactions, the mean-field Hamiltonian does not distinguish between the two sublattices. Consequently, alternate peaks in the $[00L]$ scans, figures 1 and 2, should have zero intensity for the magnetic structures suggested in table 1. We can obtain non-zero intensity for these peaks by interchanging the triplets and quartets to give for example a (4433) structure instead of a (4343) structure. These structures are however energetically unfavourable and furthermore give significantly different neutron diffraction intensities from those observed. This explanation of the extra peaks must therefore be rejected.

A more satisfactory explanation is that the Hamiltonian contains a term, or terms, which distinguish between the two sublattices, such as the trigonal interaction given by $\mathcal{H}_3$ in equation (6). The different possible forms of such an interaction are discussed in the appendix, and all have similiar effects. If, in the absence of these terms, the magnetic ordering is a planar cycloidal structure in the x–z plane, they cause the structure to distort in the y-direction, imparting a wobble to the cycloid as it propagates in the c-direction. These distortions have wavevectors $3q_c+\tau_c$, and $q_c+\tau_c$. In the case of the (4343), structure $q_c = \frac{2}{7}\tau_c$, and the x- and z-components repeat after every seven layers, while the y-component repeats only after every fourteen layers. The mean-field theory was used to calculate the commensurable structures throughout the cycloidal phase, and the results are shown in figure 7 for the 2(43) and 2(4443) structures, and in table 4 for the 2(44443) structure. The correlation functions for these structures were also calculated and are compared, in figure 8, with the results derived from the corrected experimental intensities. As explained in section 2, we used the results of Habenschuss *et al* (1974), supplemented by those of Atoji (1974) to determine the intensities of the primary reflections relative to the higher harmonics. We furthermore used their careful analysis in converting these intensities into absolute amplitudes and hence in deriving the correlation functions. The agreement between the theory and the experiments clearly indicates that the calculated structures are substantially correct.

The structures were also deduced directly from the experimental correlation functions (neglecting the peaks at (001)). The intensities are proportional to the

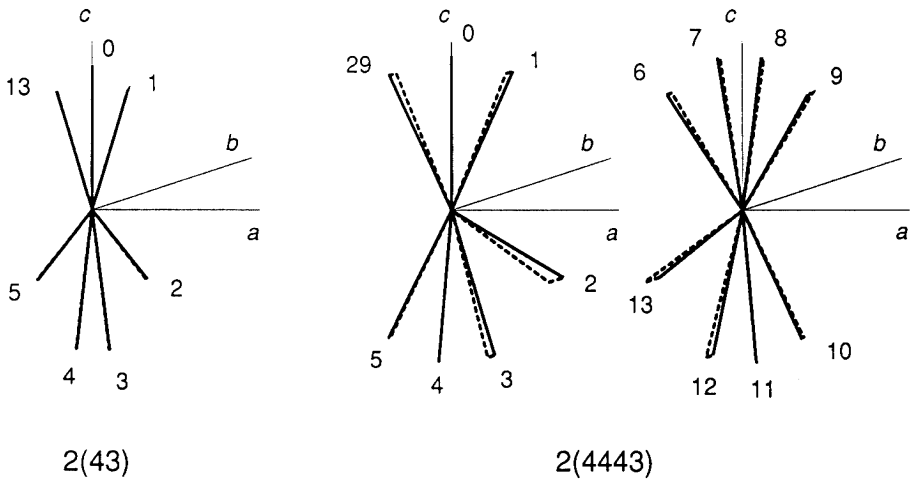

Figure 7. The structures of the 2(43) and 2(4443) phases of erbium as determined from the model at, respectively, 49 K and 35 K. The (a, b, c)-axes shown are of length $J = 7.5$, corresponding to the saturated 4f moment. The dashed lines show the projections of the angular moments on the a–c plane. The moments are labelled according to the phase convention of eqn (12), and in the remaining halves of the periodic units have the same a- and c-components but reversed b-components. This gives rise to a non-planar wobbling of the cycloid, which is small at high temperatures.

squares of the appropriate amplitudes of the Fourier expansions for the ordered moments. In general the structures cannot be obtained from the intensities without a knowledge of the phases. In all of the calculated 2(4...3) structures the ordered moments are, however, characterized by the expansions:

$$\begin{aligned}
\langle J_{xp}\rangle &= \sum_{s=1,3,\ldots} (-1)^{(s-1)/2} A_x(s) \sin[s q_c pc/2] \\
\langle J_{yp}\rangle &= \sum_{s=1,3,\ldots} (-1)^{(s-1)/2} A_y(s) \sin[s(q_c + \tau_c) pc/2] \\
\langle J_{zp}\rangle &= \sum_{s=1,3,\ldots} (-1)^{(s-1)/2} A_z(s) \cos[s q_c pc/2]
\end{aligned} \tag{11}$$

in which all the amplitudes $A_\alpha(s)$ are positive, and $s \leqslant \tau_c/q_0$. $A_z(s)$ decreases monotonically with increasing s as does $A_x(s)$ in general, while the behaviour of $A_y(s)$ is more complicated. The choice of these signs is supported by the observation that if $\langle J_{zp}\rangle = \pm J$ then $A_z(s) = 4J/\pi s$, and that the x- and y-components are smallest/largest when $\langle J_{zp}\rangle$ is largest/smallest. By using these phases, the intensities measured in our experiments and those of Habenschuss *et al.* (1974), we obtain the results shown by the circles in figure 9 for the 2(443), 2(4443) and 2(44443) structures. The comparison with the mean-field results shows that both methods give rise to very similiar structures for the J_x and J_z components. The J_y components are similar to those shown in figure 7 but are omitted from figure 9 for clarity. The main difference is that the projections of the structures on the a–c plane obtained from the experimental intensities are rather more open than those obtained from the model.

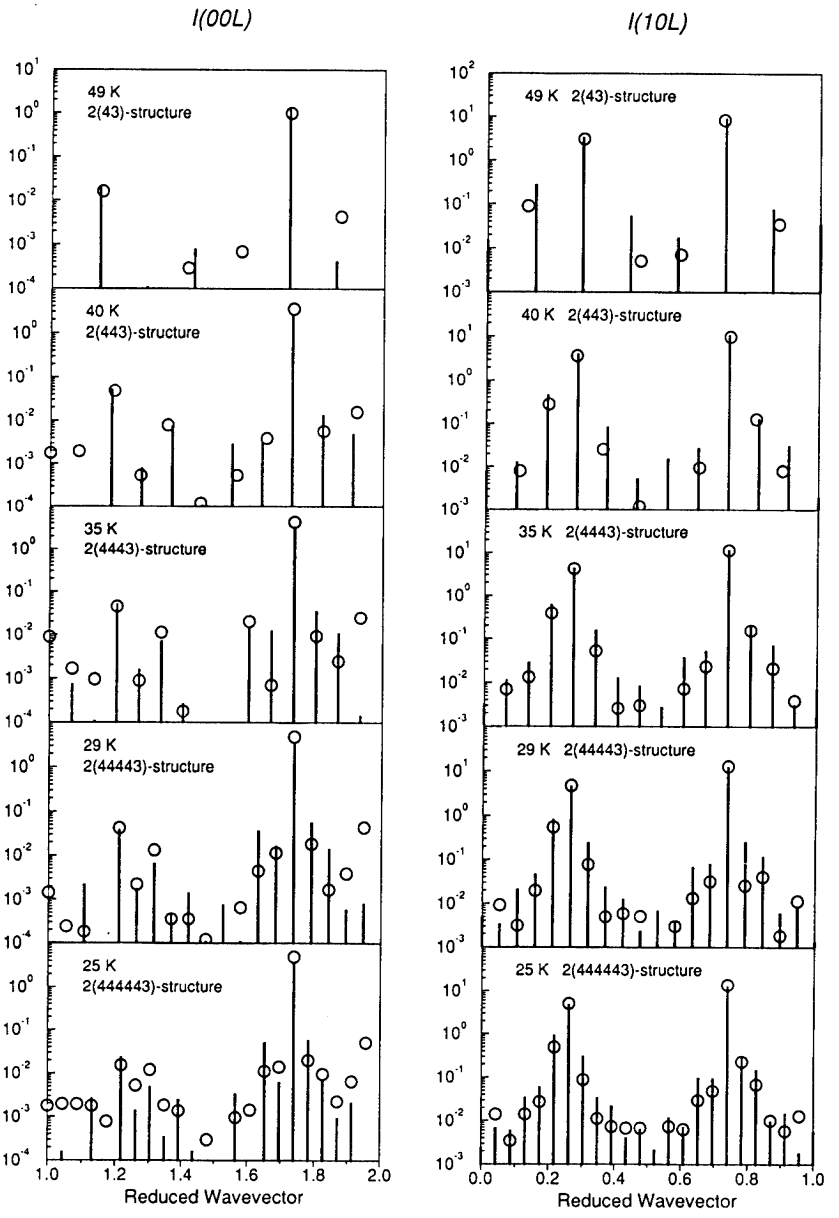

Figure 8. The correlation functions $I(00L)$ and $I(10L)$ of the commensurable magnetic structures in erbium in the intermediate cycloidal phase. The lines are derived from the calculations of the structures, and the circles are the experimental results determined from the neutron scattering intensities. The logarithmic scales in the two plots differ by one decade.

The ordered moments in a layer next to the triplet ($p = 2$ and 17 in table 4) have a large basal-plane component. At 25 K, the model predicts a tendency for this moment to jump into the basal plane to give a structure we denote as 2(4444303) instead of 2(444443). However, a comparison of the calculated intensities with the

Table 4. The 2(44443) structure at 29 K as determined from the model. The next 19 layers are identical with the first 19 given in the table, except that the signs of $\langle J_{xp} \rangle$ and of $\langle J_{zp} \rangle$ are reversed.

p	$\langle J_{xp} \rangle$	$\langle J_{yp} \rangle$	$\langle J_{zp} \rangle$
0	0.0	0.0	6.964
1	2.730	0.421	6.261
2	4.782	0.871	−3.500
3	1.910	0.474	−6.709
4	−0.651	0.018	−6.924
5	−2.891	−0.210	−6.000
6	−3.369	−0.419	5.567
7	−1.214	−0.259	6.860
8	0.897	−0.115	6.899
9	2.965	−0.077	5.899
10	2.965	0.077	−5.899
11	0.897	0.115	−6.899
12	−1.214	0.259	−6.860
13	−3.369	0.419	−5.567
14	−2.891	0.210	6.000
15	−0.651	−0.018	6.924
16	1.910	−0.474	6.709
17	4.782	−0.871	3.500
18	2.730	−0.421	−6.261

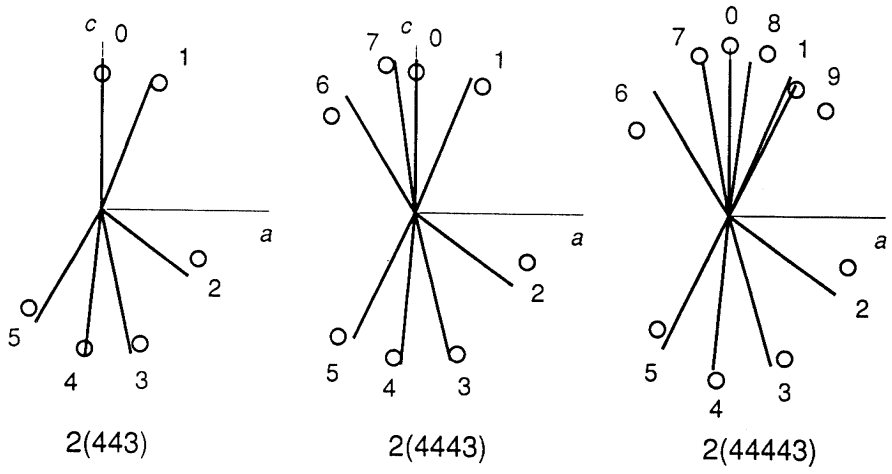

Figure 9. The structures of the 2(443), 2(4443) and 2(44443) phases. The lines are the calculated angular moments projected onto the a–c plane, and the circles are the results deduced from the experimental intensities shown in figure 8. The moments in the remaining parts of the periodic structures, which are not included, are related to those shown by simple symmetry operations.

observations clearly favours the latter structure.

The situation is more uncertain at 20 K for the eight-layered, $q_c = \frac{1}{4}\tau_c$, structure. The mean-field theory predicts that the free energies of the (3030) and the (44) structure

are nearly equal, but the scattering from these structures differs in that the third harmonic in an $[00L]$ scan is a factor of about 200 larger for the (3030) structure than for the (44) structure, so that it should be easy to distinguish between the two. However, our experimental results and those of Habenschuss *et al* (1974) give very different values for this intensity; our results shown in figure 10 favour the (3030) structure, but theirs indicate the (44) structure. We conclude that further work is needed to clarify the structure of this phase and that, since the energies of the two competing structures are very close, both may occur under different circumstances or in different crystals.

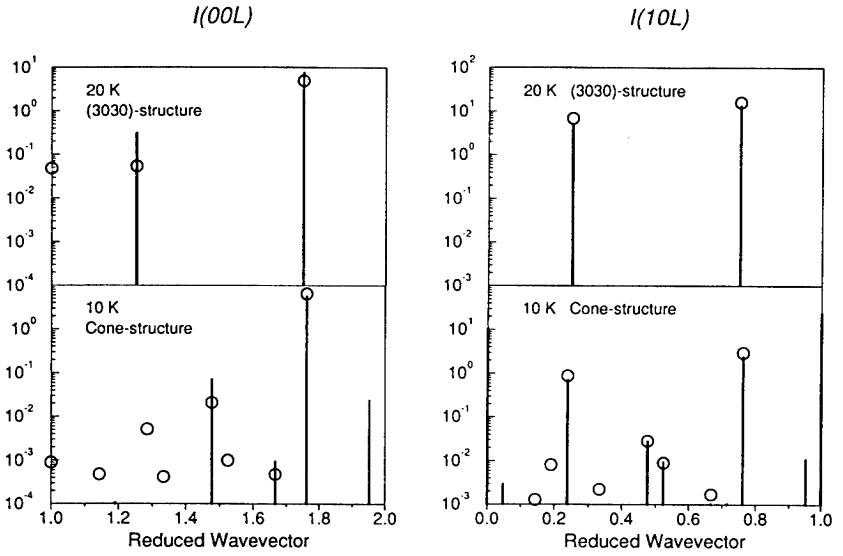

Figure 10. The correlation functions of the $\frac{1}{4}$-phase and of the cone. The meaning of the symbols is the same as in figure 8.

The experimental results obtained for the cone phase at 10 K are shown in figure 10. The ordering wave vector is $0.283\tau_c \simeq \frac{5}{21}\tau_c$, giving a period of 42 hexagonal layers. The second largest peak in the $[00L]$ scan has $q = 1.476\tau_c$, and in the $[10L]$ scan there are large peaks with $q = 0.476\tau_c$ and $0.524\tau_c$. These peaks are readily explained as arising from the effect of the trigonal coupling on the basal-plane helical ordering. If the basal-plane moments spiral uniformly, the trigonal coupling induces an anisotropy term proportional to $(-1)^p \cos 3\phi_p$, where ϕ_p is the angle between the x-axis and the basal-plane moments in the pth layer. This term leads to bunching, analogous to the effect of the single-ion hexagonal anisotropy, and thus to higher harmonics at $(3 \pm 1)q_c + \tau_c$. The model predicts not only the 2.*-harmonic at $q = 1.476\tau_c$, but also a 4.*-harmonic at $q = 1.952\tau_c$ close to the nuclear Bragg peak, which is nearly as strong but was not observed in our measurements. In contrast, Lin *et al* (1992) have clearly resolved both harmonics in the cone phase (at zero field), and a comparison shows a close agreement between their intensities for the two harmonics and those predicted by the mean-field model. We do not understand the origin of the differences between the two experiments. If, in the mean-field model, the $K_{31}^{21}(ij)$ coupling is replaced by $K_{31}^{30}(ij)$, the 2.*-harmonic is much weaker than that observed, and consequently the latter was neglected. The absence of a 5.-harmonic in both the calculations and in the measurements shows

that the single-ion hexagonal anisotropy is unimportant for the cone structure (it is effectively multiplied by $\sin^6\theta \simeq 0.01$). The trigonal coupling is therefore responsible for the lock-in of the structure at $q_c = \frac{5}{21}\tau_c$. Although the period of the commensurable structure is 42 layers, it effectively repeats itself after every 7 layers, modulus an odd/even multiple of 60° for an odd/even number of layers. This periodicity is reflected in the observed and calculated 7.-harmonic at $q = 1.667\tau_c$. This structure is shown in figure 11, which illustrates the repeat every 120°, with the moments on alternate sublattices having equivalent structures rotated by 60°. This structure is therefore a graphic illustration of the importance of the trigonal coupling and its effect in stabilizing the $\frac{5}{21}\tau_c$ wavevector. The measurements contain a number of other weak peaks, both in the $[10L]$ and the $[00L]$ scan, which are not reproduced by the model. Some of these may be due to magnetoelastic effects, the effects of which are neglected in the model, and others may be spurious. For example, peaks in the $[10L]$ scan corresponding to the one at $q = 1.286\tau_c$ in the $[00L]$ scan should have been visible, but were not observed.

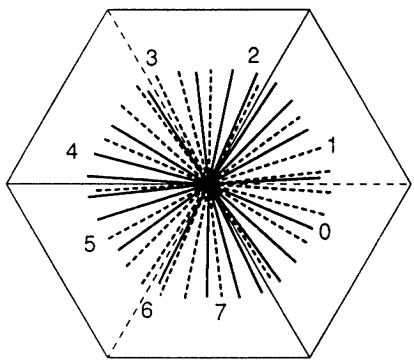

Figure 11. A projection on the basal plane of the calculated moments in the cone phase. The solid and dashed lines distinguish between the two sublattices. The moments on a particular sublattice bunch around the corresponding three a directions, leading to a pattern with a threefold rather than sixfold symmetry. The magnitude of the planar moment varies slightly, and is accompanied by a corresponding small variation of the c-axis component.

The calculated neutron diffraction intensities in general agree so completely with the experimental observations that there can be little doubt that the basic features of the structures are correct. However, there are some discrepancies, and it is difficult to judge which of them are due to failures in the model and which to experimental difficulties. In spite of the precautions which were taken, some of the weak peaks are contaminated by multiple scattering and possibly by weak contaminants in the incident beam. In addition, extinction is important. For instance, at the transition to the cone phase near 18 K, the intensity of the (100) Bragg reflection increases abruptly. We observed roughly a doubling of this intensity at the transition, while Habenschuss *et al* (1974) obtained an increase of a factor of six. The discrepancies at the highest temperatures in figure 8 may, in part, reflect that the model predicts $T_N' = 54.8$ K, whereas the experimental value seems to be higher (some 3–5 K above that reported earlier). In fact, there are indications that the basal-plane moments are ordered at even higher temperatures, but at a different wavevector from that of the c-axis component. This requires more

experimental study, as do the peaks observed at and near to [001] in many of the [00L] scans. It is hard to understand how these peaks, which have also been observed and discussed by Lin *et al* (1992), are produced by the magnetic structures. On the other hand, neither do they seem to be due to multiple scattering. It is possible that they are due to stacking faults combined with the trigonal couplings, or that the conduction electrons can produce this kind of scattering in the magnetically ordered state.

5. Conclusion

High-resolution neutron diffraction experiments and mean-field calculations have been used to determine the commensurable magnetic structures of erbium. This study illustrates very effectively the complementarity of the two techniques. Neutron diffraction alone can go far towards solving even rather complex structures, but experimental difficulties with, for example, multi-domain samples, multiple scattering and extinction, as well as the fundamental problem of phase determination, make the support of the calculations invaluable. They also suggest distortions of the structures, such as the wobbling of the cycloid and the trigonal bunching of the cone, which would be very difficult to deduce directly from the experimental data, as well as identifying the novel type of interaction which must be invoked to produce such distortions. The good agreement between the experimental and calculated diffracted intensities gives the deduced structures great credibility.

All the parameters of the model Hamiltonian, except the trigonal coupling, were obtained from magnetization and spin-wave measurements. The somewhat unsatisfactory fit to the basal-plane magnetization curve in the cone phase, shown in figure 4, makes it evident that the present model for erbium is incomplete. The basic reason is presumably that, since S is small in erbium compared with L, the RKKY exchange is relatively weak compared to other two-ion couplings and to the magnetoelastic effects. We anticipate that there are a number of additional two-ion anisotropic couplings in erbium, which have effects on the magnetic properties, but which we have not considered and are difficult to isolate.

In the intermediate phase, between the ordering temperature T_N' of the basal-plane components and T_C, the basal-plane components are not helically ordered, as originally proposed by Cable *et al* (1965). To a first approximation, the hodograph of the moments is an elliptically polarized cycloid, whose plane lies in an a–c plane of the crystal. The c-component of the ordered moments is the largest at all temperatures, and the commensurable structures are constructed from sequences of 3 or 4 successive hexagonal layers, with the c-component alternating in sign from one block to the next. This type of commensurable ordering of c-axis blocks was originally proposed by Gibbs *et al* (1986), and is confirmed, with one reservation, by the present work. From our more detailed examination of the structures, we conclude that the 3-sequences are all very similar, with the ordered moments in the second layer along the c-axis and those in the first and third layer rotated oppositely an equal angle away from the c-axis, like the layers 29–0–1 in figure 7. The four different ordered moments in a 4-sequence, surrounded by other quartets, are also arranged (approximately) symmetrically with respect to the c-axis, as the layers 6–9 in figure 7, whereas a 4-sequence next to a 3-sequence is distorted. The triplet induces a large rotation of the moments towards the basal plane in the layer closest to the triplet, and because of the hexagonal anisotropy, there is a tendency for these moments to jump into the

plane, creating a 0-layer with no ordered c-axis moment. This tendency increases with decreasing temperature, and our calculations and experiments indicate that the eight-layered structure at 20 K is more likely to be (3030) rather than (44), whereas the structures studied at higher temperatures do not seem to involve any 0-layers.

The planar arrangement of the moments in the cycloidal intermediate phase, between T'_N and T_C, is only an approximation. The experiments show clearly that the magnetic structures depend on the two different orientations of the hexagonal layers in the HCP lattice. The smallest effective reciprocal lattice vector along the c-axis, reflected in the magnetic peak positions in the $[00L]$ scans, has the length τ_c and not twice this value. This can only be explained by a trigonal coupling in the magnetic Hamiltonian, and the possible couplings of this type were established in a systematic way using general symmetry arguments. Such interactions induce a simultaneous ordering of the b-component with the a-component at T'_N, whose magnitude is proportional to the square of the a-component, to leading order. The basic ordering vector of the b-moment is $q = 3q_c + \tau_c$, and gives rise to the harmonics in the $[00L]$ scans with $q = \pm(2p+1)q_c + n\tau_c$ with odd values of n, whereas the a-component is responsible for the even-n harmonics. In accordance with equation (11) the largest displacements along the b-axis occur for the moments in the 4-blocks closest to a 3-block, as shown in figure 7 and table 4. The difference in the ordering wavevectors of the two basal-plane components means that the magnetic structure is essentially non-planar, and forms a wobbling cycloid. In the case of the eight-layered structure, the two kinds of harmonics coincide, and the (3030) and (44) structures are calculated to be only weakly non-planar. Consequently, the (44) structure is, to a good approximation, a tilted rather than a wobbling cycloid. We note that the trigonal coupling is cancelled out if the ellipsoid of the ordered moments is parallel to the b–c mirror-plane of the HCP lattice, and does not therefore produce any distortion of a cycloidal structure in this plane.

This is not the first time that trigonal couplings in the rare-earth metals have been considered, but it is the first time that unambiguous features of the magnetic structures have required such low-symmetry couplings for their explanation. In their study of the commensurable spin-slip structures in the helical phase of holmium, Cowley and Bates (1988) observed some weak peaks which suggested a modulated c-axis component superimposed on the helix. This result can be explained by the trigonal couplings (Jensen and Mackintosh 1991), since the helical components with the wavevector q_c along the c-axis induce an ordering of the c-component with $q = 3q_c + \tau_c$. In the spin-slip structures of holmium, the c-axis moment is zero at the single spin-slip planes, where the basal-plane moment is along an easy b-axis. On the pairs of planes, in which the deviation between the basal-plane moments and the nearest easy b-axis is (approximately) plus and minus the same angle, the magnitude of the c-axis component is constant but changes sign after every pair. The corresponding modulation of the c-axis component in the cone structure of erbium is calculated to be extremely weak and has not been observed. The trigonal coupling may also explain the lock-in transition to an eight-layered commensurable structure observed in holmium near 96 K (Plumer 1989, Steinitz *et al* 1989, Tindall *et al.* 1991). In the absence of the trigonal couplings, the lock-in can only be caused by the hexagonal anisotropy (possibly somewhat enhanced by a γ-strain deformation of the basal plane), and this single-ion anisotropy is very weak at such high temperatures. In the eight-layered structure with $q_c = \frac{1}{4}\tau_c$, the trigonal couplings induce a modulated c-component at $q = -3q_c + \tau_c$, which has the same wavevector as the helix. This structure is analogous

to the (3030) structure in erbium, and in holmium it is (approximately) a tilted helix, with the 0-layer moments and tilt-axis parallel to an easy b-axis. Hence, although the coupling is weak, its importance for the umklapp energy is much enhanced. If the trigonal couplings are responsible for the lock-in transition in holmium, they also offer a simple explanation for the strong enhancement of the lock-in effect observed when a magnetic field is applied in the c-direction. In this case the 4.*-modulation of the helix, which is proportional to the ferromagnetic moment along the c-axis, leads to a ferromagnetic basal-plane component ($4q_c + \tau_c = 2\tau_c$) contributing directly to the umklapp energy. Hence the trigonal couplings have the unusual effect of inducing a ferromagnetic basal-plane component in the eight-layered cone structure.

The trigonal couplings were first considered in order to explain the strong interaction between the acoustic magnons and the optical transverse phonons observed in the c-direction of Tb (Jensen and Houmann 1974). Their analysis shows that this dynamical interaction is a consequence of a coupling with threefold symmetry, and that the coupling depends on a non-collinear polarization of the conduction electrons, because it is found to involve the transverse phonons polarized orthogonal to those predicted in the case of a pure ferromagnet. Liu (1972) also concluded that the acoustic–optical interaction must derive directly from the spin–orbit coupling of the conduction electrons. His arguments are straightforwardly generalized to produce the trigonal couplings which we have considered from the spin–orbit coupling of the conduction electrons, and these interactions are equivalent to the antisymmetric Dzyaloshinsky–Moriya interaction in the magnetic transition metals. The spin–orbit effects on the band electrons in the rare-earth metals are stronger than in the transition metals and the localized moments in the rare earths (except Gd) have a large orbital component. The combination of these two factors may explain why the trigonal couplings in the rare-earth metals are relatively much larger than the very weak Dzyaloshinsky–Moriya interactions in the transition metals.

The trigonal inter-planar couplings in the model were determined from the neutron diffraction intensities. The $K_{31}^{30}(ij)$ interaction was neglected because of its weak influence on the cone structure. The two other couplings, $K_{31}^{21}(ij)$ and $K_{22}^{21}(ij)$, give similar results. We have chosen to concentrate on the first, mainly because it is a coupling between two odd-rank tensors, and thereby emphasizes that this interaction derives from the spin–orbit coupling of the conduction electrons. A model including only the inter-planar coupling $[K_{31}^{21}]_1$ between neighbouring planes leads to much larger differences between the 3.*-, 5.*- and 1.*-harmonics than observed experimentally. Consequently second and third neighbouring-plane interactions were included and the fit thereby significantly improved. The fits of the $(2p + 1)$.*-harmonics in the c-axis scans could possibly be improved further by introducing more inter-planar couplings, but most of the remaining discrepancies behave somewhat unsystematically and may be largely due to experimental difficulties. The inter-planar coupling coefficients, scaled with respect to their J-dependence, $(J - \frac{1}{2})(J - 1)[K_{31}^{21}]_n$, are comparable in magnitude to the two-ion anisotropy constants $(J - \frac{1}{2})^2(J - 1)^2[K_{33}^{2-2}]_n$ and are only about a factor of three smaller than the isotropic exchange $\mathcal{J}_n$. This comparison does not take account of the strong dependence of the anisotropy terms on the orientation of the moments. The contribution of the trigonal coupling to the energy of the different structures is at least a factor of 100 smaller than the exchange energy. Nevertheless, the trigonal coupling in erbium is surprisingly large relative to the RKKY interaction, and its magnitude

emphasizes again that a first-principles explanation of the relative magnitudes of the various magnetic interactions in the rare-earth metals is still lacking.

Acknowledgments

We are grateful to A R Mackintosh for a number of useful discussions and comments, and to D A Jehan and K N Clausen for help with some confirmatory experiments at Risø. RAC is grateful for the hospitality at the Oak Ridge National Laboratory. Financial support at Oak Ridge was provided by the US Dept. of Energy and at Oxford by the Science and Engineering Research Council.

Appendix

In this appendix symmetry arguments are used to obtain a general form for the magnetic Hamiltonian when the moments are localized on an HCP lattice. The method used is the same as that of Jensen and Houmann (1975) in their discussion of the magnon–phonon interaction in terbium. We consider only the case where the magnetic moments are the same throughout a single hexagonal layer perpendicular to the c-axis, and derive a general Hamiltonian from the completeness and the relatively simple transformation properties of the Racah operators, $\tilde{O}_{lm}$ (see the review by Lindgård and Danielsen (1974)). We assume that only *axial* tensors contribute. *Polar* tensors vanish for the isolated ions, but may in principle be non-zero in the HCP metals, because the surroundings lack inversion symmetry. They occur then because of odd-parity configuration-mixing of the 4f wavefunctions, which should be insignificant for the ground-state multiplet.

The combination of the requirements that the Hamiltonian should be Hermitian, $(c\tilde{O}_{lm})^\dagger = c^*(-1)^m\tilde{O}_{l\,-m}$, and invariant with respect to time reversal, $c\tilde{O}_{lm} \rightarrow (-1)^l(c\tilde{O}_{lm})^\dagger$, implies that a general term in the Hamiltonian may be written

$$\mathcal{H} = \sum_{ij}[\tilde{K}_{ll'}^{mm'}(ij)\tilde{O}_{lm}(i)\tilde{O}_{l'm'}(j) + (-1)^{m+m'}\tilde{K}_{ll'}^{mm'}(ij)^*\tilde{O}_{l\,-m}(i)\tilde{O}_{l'\,-m'}(j)] \tag{A1}$$

where $l + l'$ must be even. The axial tensor operators transform as follows:

$$\begin{aligned}
&\{\mathrm{I}\}\tilde{O}_{lm} = \tilde{O}_{lm}\\
&\{\mathrm{C}_z^\phi\}\tilde{O}_{lm} = \mathrm{e}^{\mathrm{i}m\phi}\tilde{O}_{lm}\\
&\{\sigma_x\}\tilde{O}_{lm} = \{\mathrm{C}_{2x}\}\tilde{O}_{lm} = (-1)^l\tilde{O}_{l\,-m}\\
&\{\sigma_y\}\tilde{O}_{lm} = \{\mathrm{C}_{2y}\}\tilde{O}_{lm} = (-1)^{l+m}\tilde{O}_{l\,-m}\\
&\{\sigma_z\}\tilde{O}_{lm} = \{\mathrm{C}_{2z}\}\tilde{O}_{lm} = (-1)^m\tilde{O}_{lm}
\end{aligned} \tag{A2}$$

where $\{\mathrm{I}\}$ is the inversion operator, $\{\sigma_x\}$ is a reflection in the plane perpendicular to the x-axis, $\{\mathrm{C}_{2x}\}$ is a rotation by π around the x-axis, and $\{\mathrm{C}_z^\phi\}$ is a rotation around the z-axis by an angle ϕ.

For the HCP structure with uniform hexagonal layers, the c-axis is a threefold axis, and when the x-, y-, or z-axes are parallel respectively to the a-, b-, or c-axis of the lattice, the Hamiltonian (A1) is invariant with respect to the application of $\{C_z^{2\pi/3}\}$, to give

$$m + m' = 3p \qquad p = 0, 1, 2, \ldots . \tag{A3}$$

The $(p = 0)$-terms include the isotropic exchange, the anisotropic interaction $K_{33}^{2-2}(q)$, and the axial crystal-field anisotropy, whereas the hexagonal crystal-field anisotropy is a $(p = 2)$-term. We shall not consider these contributions further but concentrate on the terms for which p is odd, or more specifically on the case $p = 1$ or $m + m' = 3$.

Introducing $(-1)^{m+m'} = -1$ in (A1) and using that the plane perpendicular to an a-axis, or $\{\sigma_x\}$, is a symmetry element, we obtain

$$\{\sigma_x\}\mathcal{H} = \sum_{ij}(-1)^{l+l'}\left[\tilde{K}_{ll'}^{mm'}(ij)\tilde{O}_{l\,-m}(i)\tilde{O}_{l'\,-m'}(j) - \tilde{K}_{ll'}^{mm'}(ij)^*\tilde{O}_{lm}(i)\tilde{O}_{l'm'}(j)\right] = \mathcal{H}. \tag{A4}$$

Since $l + l'$ is even, this implies that $\tilde{K}_{ll'}^{mm'}(ij)$ is purely imaginary,

$$\tilde{K}_{ll'}^{mm'}(ij)^* = -\tilde{K}_{ll'}^{mm'}(ij) \tag{A5}$$

and the resulting Hamiltonian may be written as $\mathcal{H} = \sum_{ij}\mathcal{H}(ij)$ with

$$\mathcal{H}(ij) = \tilde{K}_{ll'}^{mm'}(ij)\left[\tilde{O}_{lm}(i)\tilde{O}_{l'm'}(j) + \tilde{O}_{l\,-m}(i)\tilde{O}_{l'\,-m'}(j)\right]. \tag{A6}$$

The hexagonal layers are mirror planes of the lattice. A reflection with respect to the layer in which the ith ion is situated implies that $(i, j) \rightarrow (i, \bar{j})$, and hence that

$$\mathcal{H}(i, j) = \{\sigma_z\}\mathcal{H}(i, \bar{j}) = -\mathcal{H}(i, \bar{j})$$

or

$$\tilde{K}_{ll'}^{mm'}(i, \bar{j}) = -\tilde{K}_{ll'}^{mm'}(i, j). \tag{A7}$$

In the following, the indices 1 and 2 label the two HCP sublattices and $(\alpha, \beta) = (1, 2)$ or $(2, 1)$. The HCP lattice is invariant under a translation plus a rotation by π (or $\pi/3$) around the c-axis, in which operation $(i_1, j_\alpha) \rightarrow (i_2, j_\beta)$,

$$\mathcal{H}(i_1, j_\alpha) = \{C_{2z}\}\mathcal{H}(i_2, j_\beta) = -\mathcal{H}(i_2, j_\beta)$$

or

$$\tilde{K}_{ll'}^{mm'}(i_2, j_\beta) = -\tilde{K}_{ll'}^{mm'}(i_1, j_\alpha) \tag{A8}$$

The combination of (A7) and (A8) implies that

$$\tilde{K}_{ll'}^{mm'}(i_\alpha, j_\beta) = \tilde{K}_{ll'}^{mm'}(j_\beta, i_\alpha) \qquad \tilde{K}_{ll'}^{mm'}(i_\alpha, j_\alpha) = -\tilde{K}_{ll'}^{mm'}(j_\alpha, i_\alpha) \tag{A9}$$

showing that the coupling is symmetric in i and j, or in (lm) and $(l'm')$, when the sites belong to different sublattices, but antisymmetric if they belong to the same

sublattice. The combination of the symmetry operations used above generate the HCP lattice.

In the lowest order of $l+l' \geqslant m+m'$, i.e. for $l+l' = 4$, there are three possibilities for a trigonal coupling: $\tilde{K}^{21}_{22}$, $\tilde{K}^{30}_{31}$, and $\tilde{K}^{21}_{31}$. Introducing the Stevens operators, which are Hermitian, instead of the Racah operators, we may write the $\tilde{K}^{30}_{31}$-coupling as in equation (2.1.39) of Jensen and Mackintosh (1991). Here we consider instead the coupling $\tilde{K}^{21}_{31}$. Using $\tilde{O}_{3\pm2} = \sqrt{15}(O^2_3 \pm iO^{-2}_3)/\sqrt{8}$ and $\tilde{O}_{1\pm1} = (\mp J_x - iJ_y)/\sqrt{2}$, we obtain

$$\mathcal{H} = \mathcal{H}_3 = \sum_{ij} K^{21}_{31}(ij)[O^2_3(i)J_{yj} + O^{-2}_3(i)J_{xj}] \tag{A10}$$

where $K^{21}_{31}(ij) = (\sqrt{15}/2i)\tilde{K}^{21}_{31}(ij)$ and is real.

We have neglected the complication that the Hamiltonian (A1) in the ordered phase, where the time-reversal symmetry is broken, may contain terms proportional to $\langle \tilde{O}_{lm} \rangle$ of (mainly) magnetoelastic origin, because these terms do not change the qualitative features of the model.

References

Atoji M 1974 *Solid State Commun.* **14** 1047

Bozorth R M, Clark A E and Van Vleck J H 1972 *Int. J. Magn.* **2** 19

Cable J W, Wollan E O, Koehler W C and Wilkinson M K 1965 *Phys. Rev.* **140** A1896

Cowley R A and Bates S 1988 *J. Phys. C: Solid State Phys.* **21** 4113

Féron J L 1969 *Thesis* University of Grenoble

Coqblin B 1977 *The Electronic Structure of Rare-Earth Metals and Alloys: the Magnetic Heavy Rare-Earths* (London: Academic) figures 204–6

Gibbs D, Bohr J, Axe J D, Moncton D E and D'Amico K L 1986 *Phys. Rev.* B **34** 8182

Green R W, Legvold S and Spedding F H 1961 *Phys. Rev.* **122** 827

Habenschuss M, Stassis C, Sinha S K, Deckman H W and Spedding F H 1974 *Phys. Rev.* B **10** 1020

Lin H, Collins M F, Holden T M and Wei W 1992 *Phys. Rev.* B **45** 12873

Jensen J 1974 *J. Phys. F: Met. Phys.* **4** 1065

—— 1976 *J. Phys. F: Met. Phys.* **6** 1145

Jensen J and Houmann J G 1975 *Phys. Rev.* B **12** 320

Jensen J and Mackintosh A R 1991 *Rare Earth Magnetism. Structures and Excitations* (Oxford: Oxford University Press)

Lindgård P-A and Danielsen O 1974 *J. Phys. C: Solid State Phys.* **7** 1523

Liu S H 1972 *Phys. Rev. Lett.* **29** 793

McEwen K A, Steigenberger U and Jensen J 1991 *Phys. Rev.* **43** 3298

Miwa H and Yosida K 1961 *Prog. Theor. Phys.* **26** 693

Nagamiya T 1967 *Solid State Physics* ed F Seitz, D Turnbull and H Ehrenrich (New York: Academic) vol 20 p 305

Nicklow R M, Wakabayashi N, Wilkinson M K and Reed R E 1971 *Phys. Rev. Lett.* **27** 334

Plumer M L 1991 *Phys. Rev.* B **44** 12376

Rosen M, Kalir D and Klimker H 1973 *Phys. Rev.* B **8** 4399

Steinitz M O, Kahrizi M, Tindall D A and Ali N 1989 *Phys. Rev.* B **40** 763

Tindall D A, Steinitz M O, Kahrizi M, Noakes D R and Ali N 1991 *J. Appl. Phys.* **69** 5691